A Modified Hybrid Integral Equation to Electromagnetic Scattering from Composite PEC-Dielectric Objects Containing Closed-Open PEC Junctions

Jinbo Liu, Hongyang Chen, Hui Zhang, Jin Yuan, and Zengrui Li

State Key Laboratory of Media Convergence and School of Information and Communication Engineering
Communication University of China, Beijing, 100024, China
zrli@cuc.edu.cn

Abstract ─ To efficiently analyze the electromagnetic scattering from composite perfect electric conductor (PEC)-dielectric objects with coexisting closed-open PEC junctions, a modified hybrid integral equation (HIE) is established as the surface integral equation (SIE) part of the volume surface integral equation (VSIE), which employs the combined field integral equation (CFIE) and the electric field integral equation (EFIE) on the closed and open PEC surfaces, respectively. Different from the traditional HIE modeled for the objects whose closed and open PEC surfaces are strictly separate, the modified HIE can be applied to the objects containing closed-open junctions. A matrix equation is obtained by using the Galerkin's method of moments (MoM), which is augmented with the spherical harmonics expansion-based multilevel fast multipole algorithm (SE-MLFMA), improved by the mixed-potential representation and the triangle/tetrahedron-based grouping scheme. Because in the improved SE-MLFMA, the memory usage for storing the radiation patterns of basis functions is independent of the SIE type in the VSIE, it is highly appropriate for the fast solution of the VSIE that contains the HIE. Various numerical experiments demonstrate that during the calculation of composite objects containing closed-open PEC junctions, the application of the modified HIE in the VSIE can give reliable results with fast convergence speed.

Index Terms ─ Fast solver, integral equation, method of moments, multilevel fast multipole algorithm.

I. INTRODUCTION

In the electromagnetic analysis of composite perfect electric conductor (PEC)-dielectric objects, using the method of moments (MoM) to solve the volume surface integral equation (VSIE) is one of the most competitive approaches [1-9]. During the numerical modeling of composite objects, the electric field integral equation (EFIE) is usually formulated on all the PEC surfaces because it is independent of the surface type [2, 3], and then the EFIE is combined with the volume integral equation (VIE) established in the dielectric region to form the EFIE-VIE, a general VSIE form [2]. Whereas, when closed PEC surfaces are contained by the calculated objects, using the EFIE alone may encounter the internal-resonance problems [2, 9]. Moreover, it is typically difficult to iteratively solve the matrix equation derived from the EFIE, which is a first-kind Fredholm integral equation. To deal with the internal-resonance problems as well as to accelerate the iterative solution, some articles put forward the concept of hybrid integral equation (HIE) [4-7]. That is, establishing the combined field integral equation (CFIE) on the closed PEC surfaces of the objects [8, 9], which is the second-kind and derived from the linear combination of the EFIE and the magnetic field integral equation (MFIE), while the open surfaces keep the EFIE. Nevertheless, only the situation that the closed and open surfaces are strictly separate was discussed [4-7], while for the objects containing closed-open junctions, the traditional HIE is out of action. To overcome this drawback, the authors modified the traditional HIE to make it suitable for the PEC objects containing closed-open junctions [10]. In this paper, the modified HIE acts as the surface integral equation (SIE) part of the VSIE, combined with the VIE to form the modified HIE-VIE, a new VSIE type, to compute the composite PEC-dielectric objects that contain closed-open PEC junctions.

Using the MoM, the VSIE is converted into a matrix equation, the iterative solution process of which is usually accelerated by fast solvers such as the multilevel fast multipole algorithm (MLFMA) [2, 11-16]. Due to the addition theorem of Green's function and the diagonalization of the translation operator, the MLFMA drastically reduces the overall computational complexity from the order of $O(N^2)$ to $O(N\log N)$ through three steps: aggregation, translation, and disaggregation. To enhance the computing efficiency, the radiation patterns (RPs) of the basis functions should be computed and stored in advance. In order to minimize the sampling redundancy introduced by numerical quadrature rules, the RPs can be expanded by spherical harmonics, yielding the spherical harmonic expansion-based MLFMA (SE-MLFMA) [13-16], which is extended to the fast solution of HIE-VIE in

Submitted On: May 31, 2021
Accepted On: July 6, 2021
https://doi.org/10.47037/2020.ACES.J.360604

this paper. On the other hand, in the conventional SE-MLFMA that is dyadic form [13, 14], the memory usage of RPs is relevant to the SIE type in the VSIE. To be more specific, the memory usage costed by storing the RPs for the CFIE is double times of that for the EFIE. Therefore, if the conventional SE-MLFMA is used to accelerate the solution of HIE-VIE where the HIE is composed by the CFIE and EFIE, the RPs about the HIE are needed to be prior classified according to whether they belong to the CFIE or the EFIE part, which is quite inconvenient. To avoid this problem, this paper will adopt the improved SE-MLFMA formulated by using the mixed-potential representation [15, 16], and the RPs memory usage is then independent of the SIE type. Furthermore, the improved SE-MLFMA is grouped by a triangle/tetrahedron-based scheme, making the memory usage of RPs depend on the total number of triangles and tetrahedrons instead of the number of basis functions in the conventional SE-MLFMA. Since the total number of triangles and tetrahedrons is usually much less than that of basis functions, a considerable memory usage is saved.

The rest of this paper is organized as follows. In Section II, the modified HIE-VIE is established to be suitable for the numerical modeling of composite objects containing closed-open PEC junctions, followed by the discretization using the Galerkin's MoM. The SE-MLFMA improved by the mixed-potential representation and the triangle/tetrahedron-based grouping scheme is adopted to fast solve the HIE-VIE, which will be elaborated in Section III. Various numerical experiments are shown in Section IV to demonstrate the validity and efficiency of the proposed method. Finally, some conclusions about the application of the modified HIE-VIE are summarized.

II. DERIVATION OF THE HIE-VIE AND THE MOM SOLUTION

Suppose that in the free space, there is an electromagnetic wave $(\vec{E}^i, \vec{H}^i)$ illuminating a composite PEC-dielectric object that contains both closed and open PEC surfaces S_c and S_o as well as the dielectric region V with the permittivity ε. The scattered field $(\vec{E}^s, \vec{H}^s)$ is the superposition of fields produced by the equivalent surface and volume currents as:

$$\begin{cases} \vec{E}^s = -\left[\begin{array}{l} \mathrm{j}\omega\mu_0 \int_S \vec{J}_S(\vec{r}')G dS' + \dfrac{\mathrm{j}}{\omega\varepsilon_0}\nabla\int_S \nabla'\cdot\vec{J}_S(\vec{r}')G dS' \\ +\mathrm{j}\omega\mu_0 \int_V \vec{J}_V(\vec{r}')G dV' + \dfrac{\mathrm{j}}{\omega\varepsilon_0}\nabla\int_V \nabla'\cdot\vec{J}_V(\vec{r}')G dV' \end{array} \right] \\ \vec{H}^s = \nabla\times\int_S \vec{J}_S(\vec{r}')G dS' + \nabla\times\int_V \vec{J}_V(\vec{r}')G dV' \end{cases}, \quad (1)$$

where ε_0 and μ_0 are the permittivity and permeability of the free space, and $\vec{J}_S$ and $\vec{J}_V$ are the equivalent surface and volume currents at the source point $\vec{r}'$, respectively. With the wavenumber k and the time-harmonic factor $e^{\mathrm{j}\omega t}$, the Green's function of the free space is:

$$G = G(\vec{r}, \vec{r}') = \frac{e^{-\mathrm{j}k|\vec{r}-\vec{r}'|}}{4\pi|\vec{r}-\vec{r}'|} \quad (2)$$

In the region V, the VIE is established by making the total field equal to the sum of the incident and the scattered fields as [2]:

$$\frac{\vec{D}(\vec{r})}{\varepsilon(\vec{r})} = \vec{E}^i(\vec{r}) + \vec{E}^s(\vec{r}) \quad \vec{r}\in V, \quad (3)$$

where $\vec{D}$ is the electric flux density. By vanishing the tangential component of the total electric field on both the open and closed PEC surfaces, the EFIE based on the mixed-potential form is deduced as [2, 3]:

$$\hat{t}(\vec{r})\cdot\left[\vec{E}^s(\vec{r}) + \vec{E}^i(\vec{r})\right] = 0 \quad \vec{r}\in S_c + S_o, \quad (4)$$

where $\hat{t}$ is any tangential vector to the surface at the observation point $\vec{r}$. The EFIE is combined with the VIE to form the generally used EFIE-VIE, which is ill-conditioned at the resonant frequencies.

Imposing the boundary condition of the magnetic field over the closed PEC surface S_c, the MFIE can be established as [2, 9]:

$$\hat{n}(\vec{r})\times\left[\vec{H}^i(\vec{r}) + \vec{H}^s(\vec{r})\right] = \vec{J}(\vec{r}) \quad \vec{r}\in S_c, \quad (5)$$

where $\hat{n}$ is the outwardly directed normal. Further, similar to form the CFIE [2, 9], we can linearly combine the MFIE with the EFIE to form the so-called HIE as [4-7]:

$$\mathrm{HIE} = \alpha(\vec{r})\,\mathrm{EFIE} + \beta(\vec{r})\eta_0\,\mathrm{MFIE} \quad \vec{r}\in S_c + S_o, \quad (6)$$

where α and β are both $\vec{r}$-dependent real combined coefficients, and η_0 is the free-space intrinsic impedance. Combining the VIE and the HIE together can build the HIE-VIE, a new VSIE type. Compared with the EFIE-VIE implementation, the HIE-VIE may have a good convergence behavior when the composite objects contain closed PEC surfaces, which will be investigated during the numerical experiment. To determine the values of α and β in (6), for the traditional HIE, it is stated in [5] that $\beta(\vec{r}) = 1 - \alpha(\vec{r})$ with $0 < \alpha(\vec{r}) < 1$ for $\vec{r}\in S_c$, while $\beta(\vec{r}) = 0$ and $\alpha(\vec{r}) = 1$ for $\vec{r}\in S_o$. If the closed and open PEC surfaces of the calculated object are strictly separate, we can straightforwardly set α and β as stated above. In contrast, if the object contains closed-open junctions where the closed and open PEC surfaces have conjunct boundary, it is necessary to further discuss how to set the values of α and β.

In the initial process of the MoM, the equivalent current is expanded with basis functions. Because of the convenience of discretizing arbitrarily shaped objects and the quality of naturally avoiding pseudo line or surface charges, the divergence-conforming RWG [3] and SWG [17] basis functions based on triangular patches and tetrahedral volumes are being widely used. Using the Galerkin's MoM [1], the HIE-VIE is transformed into a generalized impedance matrix equation as:

$$\begin{bmatrix} Z^{SS} & Z^{SV} \\ Z^{VS} & Z^{VV} \end{bmatrix} \begin{Bmatrix} I^S \\ I^V \end{Bmatrix} = \begin{Bmatrix} b^S \\ b^V \end{Bmatrix}, \quad (7)$$

where $\{I^S\}$ and $\{I^V\}$ are the subvectors of unknown expansion coefficients, $\{b^S\}$ and $\{b^V\}$ are the excitation subvectors, respectively. $[Z^{PQ}]$ (P, Q is S or V) denotes the impedance submatrix representing the interactions between various types of test and basis functions. Besides, the calculation of submatrices $[Z^{VS}]$ and $[Z^{VV}]$ are independent of the SIE type, which can be found in [16]. The submatrix $[Z^{SS}]$ is the same as that generated by the pure HIE, according to whose calculation the article [10] reported how to choose the values of α and β in detail. In this paper, we will discuss the same question from the calculation of $[Z^{SV}]$. The submatrix entry Z_{mn}^{SV}, denoting the interaction between the nth SWG basis function $\vec{f}_n^V$ with domain V_n and the mth RWG test function $\vec{f}_m^S$ with domain S_m, is calculated as:

$$\begin{aligned} Z_{mn}^{SV} &= \mathrm{j}\omega\mu_0 \int_{S_m} \alpha(\vec{r})\, \vec{f}_m^S(\vec{r}) \cdot \int_{V_n} \chi(\vec{r}')\, \vec{f}_n^V(\vec{r}')\, GdV'dS \\ &+ \frac{\mathrm{j}}{\omega\varepsilon_0} \int_{S_m} \alpha(\vec{r})\, \vec{f}_m^S(\vec{r}) \cdot \nabla_S \int_{V_n} \nabla' \cdot \left[\chi(\vec{r}')\, \vec{f}_n^V(\vec{r}')\right] GdV'dS \\ &+ \eta_0 \int_{S_m} \beta(\vec{r})\, \vec{f}_m^S(\vec{r}) \cdot \left\{\hat{n}(\vec{r}) \times \int_{V_n} \left[\chi(\vec{r}')\, \vec{f}_n^V(\vec{r}')\right] \times \nabla GdV'\right\} dS \end{aligned} \quad (8)$$

with

$$\chi(\vec{r}') = 1 - \frac{\varepsilon_0}{\varepsilon(\vec{r}')}, \quad (9)$$

where ∇_s denotes the surface gradient operation. It is noticed that for the second term of the right hand side in (8), the gradient operator is placed on the observation point $\vec{r}$, leading to a two-order singularity when $\vec{r}$ approaches $\vec{r}'$. To reduce the order of singularity, taking the surface Gauss theorem, the second term in the right-hand side of (8) is usually transformed as:

$$\begin{aligned} &\int_{S_m} \alpha(\vec{r})\, \vec{f}_m^S(\vec{r}) \cdot \nabla_S \int_{V_n} \nabla' \cdot \left[\chi(\vec{r}')\, \vec{f}_n^V(\vec{r}')\right] GdV'dS \\ &= \int_{S_m} \nabla_S \cdot \left[\alpha(\vec{r})\, \vec{f}_m^S(\vec{r}) \int_{V_n} \nabla' \cdot \left[\chi(\vec{r}')\, \vec{f}_n^V(\vec{r}')\right] GdV'\right] dS \\ &- \int_{S_m} \nabla_S \cdot \left[\alpha(\vec{r})\, \vec{f}_m^S(\vec{r})\right] \int_{V_n} \nabla' \cdot \left[\chi(\vec{r}')\, \vec{f}_n^V(\vec{r}')\right] GdV'dS \\ &= \int_{\partial S_m} \alpha(\vec{r}) \left[\hat{n}_{\partial S_m} \cdot \vec{f}_m^S(\vec{r})\right] \int_{V_n} \nabla' \cdot \left[\chi(\vec{r}')\, \vec{f}_n^V(\vec{r}')\right] GdV'dl \\ &- \int_{S_m} \nabla_S \cdot \left[\alpha(\vec{r})\, \vec{f}_m^S(\vec{r})\right] \int_{V_n} \nabla' \cdot \left[\chi(\vec{r}')\, \vec{f}_n^V(\vec{r}')\right] GdV'dS \end{aligned} \quad (10)$$

where ∂S_m denotes the boundary of S_m, and $\hat{n}_{\partial S_m}$ is the outer-normal direction of ∂S_m. In (10), the singularity order is degraded to one. On the other hand, it is observed that the surface divergence operator is forced on the product $\alpha(\vec{r})\vec{f}_m^S(\vec{r})$, which is then requested to be divergence conforming. Under this restriction, if the domain S_m of $\vec{f}_m^S$ just belongs to a junctional region containing both the closed surface S_c and open surface S_o, the value of $\alpha(\vec{r})$ for $\vec{r} \in S_c$ and for $\vec{r} \in S_o$ must be the same. In other words, $\alpha(\vec{r})$ should be constant everywhere. This conclusion is the same as that drew in [10]. Therefore, we set:

$$\begin{aligned} \alpha(\vec{r}) &= \alpha_0 \quad \forall \vec{r} \in S_c + S_o \\ \beta(\vec{r}) &= \begin{cases} 1-\alpha_0 & \forall \vec{r} \in S_c \\ 0 & \forall \vec{r} \in S_o \end{cases}, \end{aligned} \quad (11)$$

where α_0 is constant and $0<\alpha_0<1$. Moreover, with a constant α, the first term in the right-hand side of (10) will be cancelled out as [3]. Please note that mathematically, the values of α and β in (8) are dependent on the position of the observation point, but not the row of the matrix as [4-7]. If the closed and open PEC surfaces are separate, depending on the observation point position and the matrix row are equivalent. Nevertheless, this equivalence is invalid when the closed and open PEC surfaces are conjoint.

Substituting (11) into (6) yields the modified HIE as:

$$\text{HIE} = \begin{cases} \alpha_0 \text{ EFIE} & \forall \vec{r} \in S_o \\ \text{CFIE} = \alpha_0 \text{ EFIE} + (1-\alpha_0)\eta_0 \text{ MFIE} & \forall \vec{r} \in S_c \end{cases}. \quad (12)$$

It states that the modified HIE consists of two parts: the CFIE on the closed surface S_c, and the EFIE scaled down by multiplying a coefficient α_0 on the open surface S_o. The modified HIE can be combined with the VIE to form the modified HIE-VIE for the calculation of composite objects containing closed-open PEC junctions.

III. SE-MLFMA IMPLEMENTATION

In the SE-MLFMA, the impedance matrix generated by the MoM is decomposed into two parts as $[Z_N] + [Z_F]$, where $[Z_N]$ and $[Z_F]$ denote the matrices representing the interactions between the basis and test functions in the near and far groups, respectively. In our implementation, the grouping scheme is based on triangles and tetrahedrons [15, 16], rather than the most commonly used edge-based grouping scheme [2, 11-14]. That is to say, the index of the leaf box which a given triangle or tetrahedron belongs to is determined by comparing the box center coordinate with the triangle or tetrahedron barycenter. It was reported in [16] that how to use the SE-MLFMA to accelerate the VSIE solution of EFIE-VIE type. In this section, we focus on the SE-MLFMA application on the HIE part of the HIE-VIE matrix, which is $[Z^{SS}]$.

The nth RWG basis function is defined over a common edge of length l_n shared by two adjacent triangles $T_n^{\pm}$ of areas $A_n^{\pm}$ as:

$$\vec{f}_n^S(\vec{r}') = \pm \frac{l_n}{2A_n^{\pm}} \left(\vec{r}' - \vec{r}_n^{\pm}\right), \quad (13)$$

where the sign "±" means the current flowing direction is outward or inward to $T_n^{\pm}$, and $\vec{r}_n^{\pm}$ is the free vertex of $T_n^{\pm}$ to the common edge. Since the RWG basis function is defined on two adjacent triangles, the submatrix entry Z_{mn}^{SS} consists of four double surface integrals,

$$Z_{\mathrm{F}mn}^{SS++}=\frac{l_m l_n}{4A_m^+A_n^+}\left\{\begin{array}{l}\mathrm{j}\omega\mu_0\int_{T_m^+}\alpha_0\left(\vec{r}-\vec{r}_m^{\,+}\right)\cdot\int_{T_n^+}\left(\vec{r}'-\vec{r}_n^{\,+}\right)GdS'dS-\dfrac{\mathrm{j}}{\omega\varepsilon_0}\int_{T_m^+}\nabla_S\cdot\left[\alpha_0\left(\vec{r}-\vec{r}_m^{\,+}\right)\right]\int_{T_n^+}\nabla_S'\cdot\left(\vec{r}'-\vec{r}_n^{\,+}\right)GdS'dS\\+\eta_0\int_{T_m^+}\beta_m^+\left(\vec{r}-\vec{r}_m^{\,+}\right)\cdot\hat{n}\left(\vec{r}\right)\times\int_{T_n^+}\left(\vec{r}'-\vec{r}_n^{\,+}\right)\times\nabla GdS'dS\end{array}\right\}$$

$$=\frac{l_m l_n k}{64A_m^+A_n^+\pi^2}\left\{\begin{array}{l}\alpha_0\omega\mu_0\oint\left[\int_{T_m^+}\left(\vec{r}-\vec{r}_m^{\,+}\right)e^{-\mathrm{j}\vec{k}\cdot\left(\vec{r}-\vec{r}_{m'}\right)}dS\right]T_L\left(\vec{k},\vec{r}_{m'n'}\right)\cdot\left[\int_{T_n^+}\left(\vec{r}'-\vec{r}_n^{\,+}\right)e^{-\mathrm{j}\vec{k}\cdot\left(\vec{r}_{n'}-\vec{r}'\right)}dS'\right]d^2\hat{k}\\-\alpha_0\dfrac{2}{\omega\varepsilon_0}\oint\left[\int_{T_m^+}e^{-\mathrm{j}\vec{k}\cdot\left(\vec{r}-\vec{r}_{m'}\right)}dS\right]T_L\left(\vec{k},\vec{r}_{m'n'}\right)\left[\int_{T_n^+}e^{-\mathrm{j}\vec{k}\cdot\left(\vec{r}_{n'}-\vec{r}'\right)}dS'\right]d^2\hat{k}\\-\beta_m^+\eta_0\oint\left\{\int_{T_m^+}\left[\hat{n}\left(\vec{r}\right)\times\left(\vec{r}-\vec{r}_m^{\,+}\right)\times\vec{k}\right]e^{-\mathrm{j}\vec{k}\cdot\left(\vec{r}-\vec{r}_{m'}\right)}dS\right\}T_L\left(\vec{k},\vec{r}_{m'n'}\right)\cdot\left[\int_{T_n^+}\left(\vec{r}'-\vec{r}_n^{\,+}\right)e^{-\mathrm{j}\vec{k}\cdot\left(\vec{r}_{n'}-\vec{r}'\right)}dS'\right]d^2\hat{k}\end{array}\right\}\tag{16}$$

$$=\frac{l_m l_n k}{64A_m^+A_n^+\pi^2}\left\{\begin{array}{l}\alpha_0\omega\mu_0\oint\left[\tilde{\vec{V}}_m^*\left(\vec{k}\right)-\vec{r}_m^{\,+}\tilde{S}_m^*\left(\vec{k}\right)\right]T_L\left(\vec{k},\vec{r}_{m'n'}\right)\cdot\left[\tilde{\vec{V}}_n\left(\vec{k}\right)-\vec{r}_n^{\,+}\tilde{S}_n\left(\vec{k}\right)\right]d^2\hat{k}\\-\alpha_0\dfrac{2}{\omega\varepsilon_0}\oint\tilde{S}_m^*\left(\vec{k}\right)T_L\left(\vec{k},\vec{r}_{m'n'}\right)\tilde{S}_n\left(\vec{k}\right)d^2\hat{k}\\-\beta_m^+\eta_0\oint\hat{n}\left(\vec{r}\right)\times\left[\tilde{\vec{V}}_m^*\left(\vec{k}\right)-\vec{r}_m^{\,+}\tilde{S}_m^*\left(\vec{k}\right)\right]\times\vec{k}T_L\left(\vec{k},\vec{r}_{m'n'}\right)\cdot\left[\tilde{\vec{V}}_n\left(\vec{k}\right)-\vec{r}_n^{\,+}\tilde{S}_n\left(\vec{k}\right)\right]d^2\hat{k}\end{array}\right\}$$

representing the mutual interactions between the four triangles involved in the basis and test functions. In the following, for the purpose of easy reading, only the integral involving two "positive" triangles is considered, and other three ones can be obtained by simply changing the signs. If two positive triangles T_m^+ and T_n^+ are grouped into the *m'*th and *n'*th leaf boxes of the centers coordinates $\vec{r}_{m'}$ and $\vec{r}_{n'}$, respectively, then via the addition theorem of Green's function, (2) is rewritten as:

$$G\left(\vec{r},\vec{r}'\right)=\frac{-\mathrm{j}k}{\left(4\pi\right)^2}\oint e^{-\mathrm{j}\vec{k}\cdot\left(\vec{r}-\vec{r}_{m'}\right)}T_L\left(\vec{k},\vec{r}_{m'n'}\right)e^{-\mathrm{j}\vec{k}\cdot\left(\vec{r}_{n'}-\vec{r}'\right)}d^2\hat{k}\,,\tag{14}$$

with the translation operator [2],

$$T_L\left(\hat{k},\vec{r}_{m'n'}\right)=\sum_{l=0}^{L}\left(-\mathrm{j}\right)^l\left(2l+1\right)h_l^{(2)}\left(k\left|\vec{r}_{m'n'}\right|\right)P_l\left(\hat{k}\cdot\hat{r}_{m'n'}\right),\tag{15}$$

where $\vec{r}_{m'n'}=\vec{r}_{m'}-\vec{r}_{n'}$, L is the order of multipole expansion, $h_l^{(2)}$ is the second-kind spherical Hankel function of order l, and P_l denotes the Legendre Polynomial of degree l. In the far-group interaction, Substituting (14) and (15) into the expression of Z_{mn}^{SS} results in (16), where β_m^+ is $1-\alpha_0$ when the triangle T_m^+ belongs to the closed surface S_c, or 0 for $T_m^+\in S_o$, and the asterisk denotes the complex conjugate. It is seen that the scalar $\tilde{S}_\beta$ and vector $\tilde{\vec{V}}_\beta$ with:

$$\left\{\begin{array}{l}\tilde{S}_\beta\left(\vec{k}\right)=\int_{T_\beta^+}e^{-\mathrm{j}\vec{k}\cdot\left(\vec{r}_{\beta'}-\vec{r}'\right)}dS'\\\tilde{\vec{V}}_\beta\left(\vec{k}\right)=\int_{T_\beta^+}\vec{r}'e^{-\mathrm{j}\vec{k}\cdot\left(\vec{r}_{\beta'}-\vec{r}'\right)}dS'\end{array}\right.\quad\beta=m,n\,,\tag{17}$$

contain all information needed by the aggregation and disaggregation processes in the leaf boxes in the MLFMA, which means that they can be regarded as the RPs defined on triangles. Using the symmetry of RPs, the memory usage in bytes by storing the RPs is:

$$\mathrm{Mem}_{\mathrm{RP}}=4cN_{\mathrm{t}}\left(L+1\right)^2\quad c=\left\{\begin{array}{ll}8 & \text{single precision}\\16 & \text{double precison}\end{array}\right.,\tag{18}$$

where N_{t} is the number of triangles.

Further, in the improved SE-MLFMA [15, 16], the RPs of triangles can be expressed as a series of the spherical harmonics as:

$$\left\{\begin{array}{l}\tilde{S}_\beta\left(\vec{k}\right)=\sum_{p=0}^{P}\sum_{q=-p}^{p}S_{pq}^{\beta}Y_{pq}\left(\hat{k}\right)\\\tilde{\vec{V}}_\beta\left(\vec{k}\right)=\sum_{p=0}^{P}\sum_{q=-p}^{p}\vec{V}_{pq}^{\beta}Y_{pq}\left(\hat{k}\right)\end{array}\right.,\tag{19}$$

where Y_{pq} is the orthonormalized spherical harmonics [18]. The expansion coefficients are computed by:

$$\left\{\begin{array}{l}S_{pq}^{\beta}=\int\tilde{S}_\beta\left(\vec{k}\right)Y_{pq}^*\left(\hat{k}\right)d^2\hat{k}\\\vec{V}_{pq}^{\beta}=\int\tilde{\vec{V}}_\beta\left(\vec{k}\right)Y_{pq}^*\left(\hat{k}\right)d^2\hat{k}\end{array}\right..\tag{20}$$

Instead of the RPs, the expansion coefficients S_{pq}^{β} and $\vec{V}_{pq}^{\beta}$ can be computed and stored in the setup of the improved SE-MLFMA, while the memory usage in bytes is:

$$\mathrm{Mem}_{\mathrm{SE}}=2cN_{\mathrm{t}}\left(P+1\right)\left(P+2\right),\tag{21}$$

where P is the degree of spherical harmonics. Usually, $P = L/2 - 1$ is recommended with an sufficient accuracy. Thus, compared (21) with (18), a large amount of memory usage is saved.

The above content discussed how to apply the SE-MLFMA on the $[Z^{SS}]$ part of (7), while the similar application about other three parts $[Z^{SV}]$, $[Z^{VS}]$ and $[Z^{VV}]$ is shown in [16]. The remaining steps, such as the computation of expansion coefficients as well as aggregation and disaggregation steps at the finest level using the spherical harmonics series, are done in the same way as [14-16]. The analysis on advantages of the

improved SE-MLFMA have been given in [15, 16], which are beyond the scope of this paper. But we still summarize them as follows:

1) The memory requirement does not depend on the SIE type, which means that the application of HIE-VIE will not cause any memory increasing compared with the EFIE-VIE implementation. Because of the adoption of mix-potential representation, the complex conjugate of (17) can be reused as the receiving patterns for any SIE type in the disaggregation step, which is impossible for the dyadic-form MLFMA when the MFIE is involved.
2) The memory requirement of RPs is only proportional to the total number of triangles and tetrahedrons rather than that of the basis functions, leading to a considerable reduction of core memory requirement. This is due to the grouping scheme based on the triangles and tetrahedrons [15, 16], rather than the commonly edge-based grouping scheme [2, 11-14].
3) Compared with the conventional SE-MLFMA, the improved one has a faster execution. Since in the improved SE-MLFMA, the Cartesian components of RPs are permanently used during the whole procedures, the repeated transforms between Cartesian and spherical coordinates, which is inevitable for the conventional SE-MLFMA to eliminate the Gibbs phenomenon [13, 14], are totally eliminated.

IV. NUMERICAL EXPERIMENTS

In the following, the bistatic radar cross section (RCS) results of several objects at $0 \le \theta \le 180°$ and $\varphi = 0$ are calculated, all of which are illuminated by an x-polarized plane wave from $+z$-axis. The generalized minimal residual algorithm (GMRES) with a restart number 100 is adopted as the iterative solver to reach 0.001 relative residual error [19]. The constant α_0 in (11) is 0.5. Unless otherwise stated, the leaf box size of the MLFMA is fixed to 0.25λ, in which situation the degree of spherical harmonics $P = 2$ with the order of multipole expansion $L = 5$. During the HIE-VIE modeling for the composite objects containing closed-open PEC junctions, the CFIE is established on the closed PEC surface, and the EFIE is on the remaining open surface. All the calculations serially execute on a computer with 3.2 GHz CPU and 16 GB RAM in single precision.

The first case is a composite object, which is a closed semisphere of radius 5λ coated with 0.05λ thickness material from the top surface, midmost clung to an open square plate of variable side length l, as shown inside Fig. 1 (a). The relative permittivity of the coating material is $\varepsilon_r = 2.2 - j0.00198$. A moderate mesh size is chosen to discretize the object, while the numbers of triangles and unknowns with respect to different values of l are given in Table 1. Besides, the numbers of tetrahedrons and the triangles belonging to the closed semisphere are fixed to 118,401 and 59,960, respectively.

The numerical results from the EFIE-VIE and the modified HIE-VIE with $l = 10\lambda$ and $l = 30\lambda$ are shown in Figs. 1 (a) and (b). The traditional HIE-VIE result, i.e., $\alpha(\vec{r})$ is 0.5 for $\vec{r} \in S_c$ and 1 for $\vec{r} \in S_o$, is also given. It is observed that the results from EFIE-VIE and modified HIE-VIE are in agreement everywhere, while the result from traditional HIE-VIE shows a totally unacceptable difference. This phenomenon states the necessity of modifying the traditional HIE. In order to investigate how the proportion of the closed PEC surface occupying the whole PEC structure of the composite object influences the performance of the modified HIE-VIE or the EFIE-VIE, Fig. 2 shows the number of iterations with respect to various l. It is observed that when $l = 10\lambda$, the coverage speed of the HIE-VIE is about 2.6 times faster than the EFIE-VIE (iterations 231 vs. 601). Along with the increase of l, the number of iterations from the HIE-VIE will sharply increase, while that from the EFIE-VIE is relatively stable. This phenomenon illuminates that the HIE-VIE can be more efficient for the calculation in which the closed surface occupies a main proportion of the whole PEC structure. On the other hand, the iteration number from the HIE-VIE is always less than the EFIE-VIE. Therefore, we may draw the conclusion that no matter what the proportion of the closed PEC surface in the whole object is, the HIE-VIE can always be adopted safely and reliably.

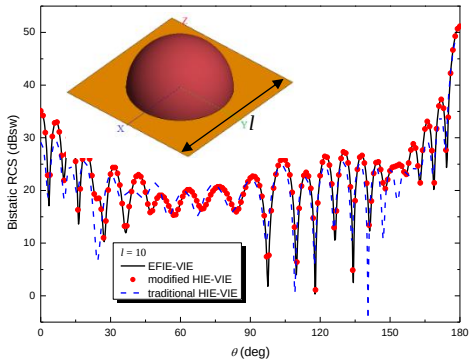

(a) l=10λ

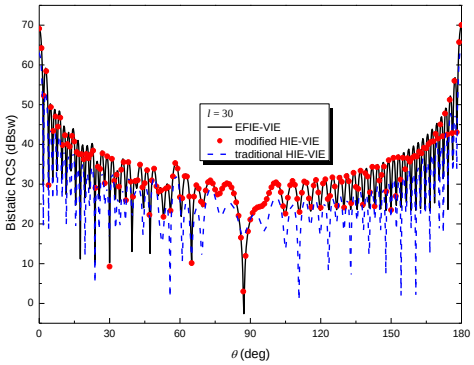

(b) l=30λ

Fig. 1. Bistatic RCS results from a coated semisphere of radius 5λ clung to a square plate of side length l.

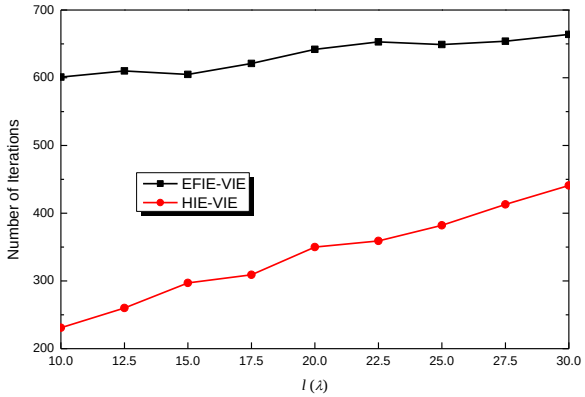

Fig. 2. Numbers of iterations with respect to various l in the calculation of the composite object shown inside Fig. 1 (a), while the GMRES with 100 restart number is the iterative solver to reach 0.001 relative residual error.

Table 1: Numbers of triangles and unknowns with respect to different values of l

***l* (λ)**	**Number of Triangles**	**Number of Unknowns**
10	64,298	373,270
12.5	76,736	391,008
15	91,612	413,713
17.5	109,991	441,320
20	131,317	473,253
22.5	156,119	510,397
25	183,805	551,875
27.5	214,801	597,272
30	247,065	646,698

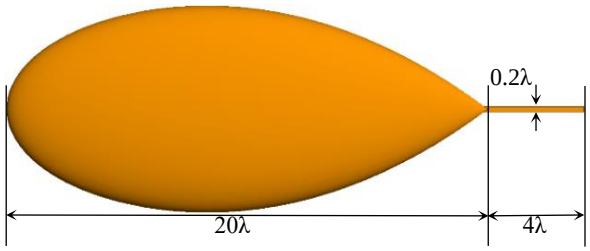

Fig. 3. An almond of length 20λ, penetrated by a narrow strip from the tip, whose width is 0.2λ, and the length from the tip of the almond is 4λ.

Table 2: Memory usage of RPs and CPU time per MVP versus different L and P

Box Size	Method	Parameter	*RP Mem* (MB)	MVP Time (s)	
				EFIE	HIE
0.25λ	*Trad*	L=5	67.40	0.592	0.662
	Imp	P=2	11.23	0.506	0.532
		P=3	18.72	0.539	0.561
0.3λ	*Trad*	L=6	91.73	0.721	0.895
	Imp	P=2	11.23	0.538	0.575
		P=3	18.72	0.575	0.619

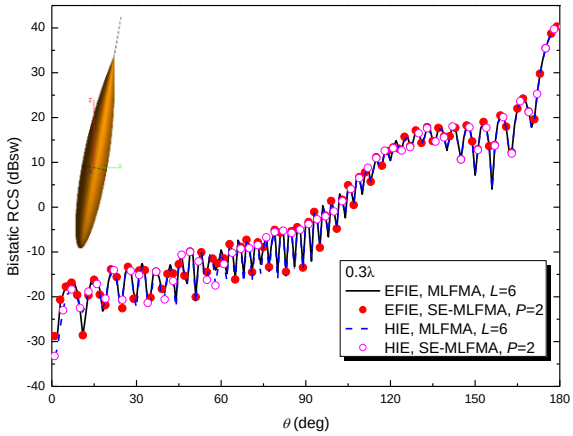

Fig. 4. Bistatic RCS results from the object shown in Fig. 3, with an intersection angle of 10° between the axis of the almond and +z-axis.

The second object is a pure-PEC almond of length 20λ [20], penetrated by a narrow strip from the tip, as shown in Fig. 3. The width of the strip is 0.2λ, while the length from the tip of the almond is 4λ. In order to make the incident plane wave illuminate the closed-open PEC junction structure adequately, in which situation whether the junction structure is properly modeled or not will have a strong influence on the RCS results, there is an intersection angle of 10° between the axis of the almond and +z-axis as shown inside Fig. 4. This object is discretized into 92,126 unknowns, while the numbers of triangles belonging to the closed almond and the open strip are 61,200 and 145, respectively. In this case, the pure SIE methods, EFIE and HIE, are used to model the object. To illustrate the effectiveness of the improved SE-MLFMA, both the traditional MLFMA and the improved SE-MLFMA are used, while two kinds of leaf box sizes (0.25λ with L=5 and 0.3λ with L=6) in the MLFMA are adopted during the calculation, respectively. Please note in our implementation, the traditional MLFMA is also expressed by the mixed-potential representation and grouped based on the triangles, thus, the memory usage of RPs is independent of the SIE type and in proportion to the number triangles. Table 2 gives the detail information on the memory usage of RPs (*RP Mem*) and the CPU time per matrix-vector product (MVP time) during the iterative solution with different SIE type (EFIE or HIE). It is observed that compared with the traditional MLFMA (*trad*), the improved SE-MLFMA (*imp*) saves a considerable core memory usage, matching with (18) or (21). Besides, the improved SE-MLFMA is even faster than the traditional MLFMA in the MVP implementation. This is because the aggregation of the outgoing waves and the disaggregation of the incoming waves at the finest level can be computed in an efficient way by summation of the spherical harmonics instead of the integrations. When the leaf box size is 0.3λ, the EFIE

and HIE are used to calculate the bistatic RCS results accelerated by the MLFMA with L=6 and SE-MLFMA with P=2, respectively, which are displayed in Fig. 4. Excellent agreements are observed, indicating that although the sharp tips and edges are contained, the results from the HIE are also dependable, while the formula $P = L/2 - 1$ can still provide an acceptable accuracy for the HIE accelerated by the SE-MLFMA. During the calculation, the numbers of iteration from the HIE and EFIE are 76 and 712, respectively. Since in this example, the closed almond part occupies an absolutely large proportion of the whole object, the advantage of HIE to the EFIE on the convergence speed is quite clear.

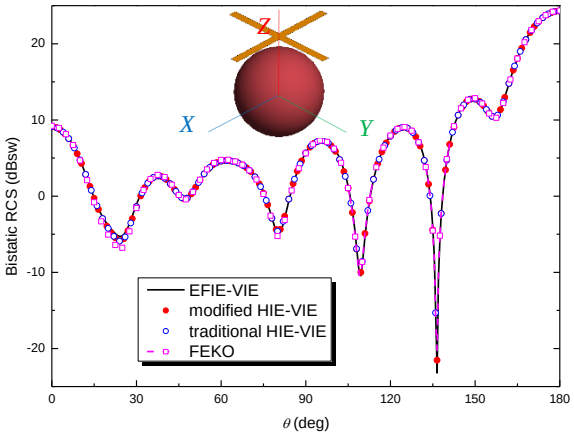

Fig. 5. Bistatic RCS results from composite object. The radius of PEC sphere is 1λ, the thickness of the coating material is 0.05λ with $\varepsilon_r = 3.35$, and the distance between the PEC cross and the center of sphere is 1.5λ.

The third case is a composite object. A PEC cross, each branch size of which is 3λ × 0.2λ, is placed over a coated sphere, as shown inside Fig. 5. The radius of PEC sphere is 1λ, the thickness of the coating material is 0.05λ with $\varepsilon_r = 3.35$, and the distance between the PEC cross and the center of sphere is 1.5λ. With a 0.07λ average mesh size, this object is discretized into 55,135 unknowns with 6,160 closed triangles, 322 open triangles and 19,570 tetrahedrons. In this case, since the closed and open PEC surfaces are totally separate, both the traditional HIE-VIE and the modified one can be adopted safely. The bistatic RCS results from the EFIE-VIE, the traditional HIE-VIE and the modified HIE-VIE implementations are shown in Fig. 5, while for comparison, the result from the electromagnetic simulation commercial software Altair FEKO using the SIE-based method is also shown [21]. Good agreement is observed among them. The iteration number from the modified HIE-VIE is 103, almost equal to 106 that is from the traditional one, and about 2.7 times faster than that from the EFIE-VIE which is 280. This case states that for the composite objects whose closed and open PEC surfaces are separate, the modified HIE-VIE can also give reliable result and has a similar convergence behavior compared with the traditional one. In other words, the modified HIE implementation is always effective on reducing the iteration number for any kind of composite objects without losing the numerical accuracy.

V. CONCLUSIONS

The modified HIE is combined with the VIE to form the HIE-VIE, a new VSIE type, to exactly model the composite PEC-dielectric objects that contain closed-open PEC junctions. For the SIE part of the VSIE, different from the traditional HIE establishing for objects whose closed and open PEC surfaces are strictly separate, in the modified HIE, the combined coefficient α multiplied the EFIE in (6) must be constant everywhere. Compared with the EFIE-VIE implementation, the use of modified HIE-VIE can always improve the efficiency of the iterative solution to some extent with a high accuracy. The validity and efficiency are verified by various numerical experiments, while during the calculation, the improved SE-MLFMA, whose memory usage for storing the RPs is independent of the SIE type, is used to accelerate the iterative solution.

ACKNOWLEDGMENT

This work was supported by the National Natural Science Foundation of China (Grant Numbers 62071436 and 61971384), and the Fundamental Research Fund for the Central Universities (Grant Numbers CUC210B013 and CUC19ZD001).

REFERENCES

[1] R. F. Harrington, *Field Computation by Moment Methods*. MacMillan, New York, 1968.

[2] W. C. Chew, J. M. Jin, E. Michielssen, and J. M. Song, *Fast and Efficient Algorithms in Computational Electromagnetics*. Boston, MA, USA: Artech House, 2001.

[3] S. M. Rao, D. R. Wilton, and A. W. Glisson, "Electromagnetic scattering by surfaces of arbitrary shape," *IEEE Trans. Antennas Propag.*, vol. 30, no. 3, pp. 409-418, May 1982.

[4] L. Gürel and Ö. Ergül, "Extending the applicability of the combined-field integral equation to geometries containing open surfaces," *IEEE Antennas Wireless Propag. Lett.*, vol. 5, pp. 515-516, 2006.

[5] Ö. Ergül and L. Gürel, "Iterative solutions of hybrid integral equations for coexisting open and closed surfaces," *IEEE Trans. Antennas Propag.*, vol. 57, no. 6, pp. 1751-1758, June 2009.

[6] Z. H. Fan, D. Z. Ding, and R. S. Chen, "The efficient analysis of electromagnetic scattering from composite structures using hybrid CFIE-

IEFIE," *Progress in Electromagnetics Research B*, vol. 10, pp. 131-143, 2008.

[7] B. Karaosmanoğlu, C. Önol, and Ö. Ergül, "Optimizations of EFIE and MFIE combinations in hybrid formulations of conducting bodies," *in 2015 International Conference on Electromagnetics in Advanced Applications (ICEAA)*, Turin, Italy, Oct. pp. 1276-1279, 2015.

[8] J. R. Mautz and R. F. Harrington, "H-field, E-field and combined-field solutions for conducting bodies of revolution," *Arch. Elektron. Übertragungstech. (Electron. Commun.)*, vol. 32, pp. 157-164, 1978.

[9] P. Ylä-Oijala and M. Taskinen, "Calculation of CFIE impedance matrix elements with RWG and n×RWG functions," *IEEE Trans. Antennas Propag.*, vol. 51, no. 8, pp. 1837-1846, Aug. 2003.

[10] J. Liu, J. Yuan, W. Luo, Z. Li, and J. Song, "On the use of hybrid CFIE-EFIE for objects containing closed-open surface junctions," *IEEE Antennas Wireless Propag. Lett.*, vol. 20, no. 7, pp. 1249-1253, July 2021.

[11] S. Velamparambil, W. C. Chew, and J. M. Song, "10 million unknowns: is it that big?" *IEEE Antennas Propag. Mag.*, vol. 45, no. 2, pp. 43-58, Apr. 2003.

[12] Ö. Ergül and L. Gürel, "Rigorous solutions of electromagnetics problems involving hundreds of millions of unknowns," *IEEE Antennas Propag. Mag.*, vol. 53, no. 1, pp. 18-26, Feb. 2011.

[13] Ismatullah and T. F. Eibert, "Surface integral equation solutions by hierarchical vector basis functions and spherical harmonics based multilevel fast multipole method," *IEEE Trans. Antennas Propag.*, vol. 57, no. 7, pp. 2084-2093, July 2009.

[14] T. F. Eibert, "A diagonalized multilevel fast multipole method with spherical harmonics expansion of the k-space integrals," *IEEE Trans. Antennas Propag.*, vol. 53, no. 2, pp. 814-817, Feb. 2005.

[15] M. He, J. Liu, and K. Zhang, "Improving the spherical harmonics expansion based multilevel fast multipole algorithm (SE-MLFMA)," *IEEE Antennas Wireless Propag. Lett.*, vol. 12, pp. 551-554, 2013.

[16] J. Liu, M. He, Z. Li, and J. Su, "The application of improved spherical harmonics expansion-based multilevel fast multipole algorithm in the solution of volume-surface integral equation," *Int. J. Antenn. Propag.*, vol. 2018, 7 pages, Apr. 2018.

[17] D. H. Schaubert, D. R. Wilton, and A. W. Glisson, "A tetrahedral modeling method for electromagnetic scattering by arbitrarily shaped inhomogeneous dielectric bodies," *IEEE Trans. Antennas Propag.*, vol. 32, no. 1, pp. 77-85, Jan. 1984.

[18] R. F. Harrington, *Time Harmonic Electromagnetic Fields*. New York: McGraw-Hill, 1961.

[19] Y. Saad and M. H. Schultz, "GMRES: A generalized minimal residual algorithm for solving nonsymmetric linear systems," *SIAM J. Sci. and Stat. Comput.*, vol. 7, no. 3, pp. 856-869, 1986.

[20] A. C. Woo, H. T. G. Wang, M. J. Schuh, and M. L. Sanders, "EM programmer's notebook-benchmark radar targets for the validation of computational electromagnetics programs," *IEEE Antennas Propag. Mag.*, vol. 35, no. 1, pp. 84-89, Feb. 1993.

[21] Altair. (2014). FEKO, Suite 7.0 [Online]. Available: http://www.feko.info